5-1-2005

Intrinsically biased electrocapacitive catalysis

D. P. Sheehan
University of San Diego, dsheehan@sandiego.edu

T. Seideman
Northwestern University

Intrinsically biased electrocapacitive catalysis

D. P. Sheehan[a)]
Department of Physics, University of San Diego, San Diego, California 92110

T. Seideman
Department of Chemistry, Northwestern University, Evanston, Illinois 60208

(Received 27 December 2004; accepted 22 March 2005; published online 27 May 2005)

We propose the application of the contact potential from metal-metal junctions or the built-in potential of semiconductor *p-n* junctions to induce or catalyze chemical reactions. Free of external sources, this *intrinsic* potential across microscale and nanoscale vacuum gaps establishes electric fields in excess of 10^7 V/m. The electrostatic potential energy of these fields can be converted into useful chemical energy. As an example, we focus on the production of superthermal gas ions to drive reactions. Analysis indicates that this *intrinsically biased electrocapacitive catalysis* can achieve locally directed ion energies up to a few electron volts and local gas temperature boosts in excess of 10^4 K. Practical considerations for implementation and experimental tests are considered. © *2005 American Institute of Physics*. [DOI: 10.1063/1.1908411]

I. INTRODUCTION

Catalytic reactions play an important role in most present day chemical manufacturing, both organic and inorganic.[1–3] Heterogeneous gas-solid catalysts, in particular, are necessary for production of essential gases (e.g., NH_4, SO_2, H_2, CO_2), for petrochemical cracking and hydrocracking, for hydrogenation, dehydrogenation, oxidation, isomerization, and polymerization of hydrocarbons. Since a large catalytic surface area is paramount, commercial catalysts typically consist of finely divided powders or are physically supported on stable, high porosity, and high surface area grains such as alumina, silica, or zeolites.

Electrochemical reactions—e.g., electrorefining, electrowinning, electroforming, electrolysis—are mostly carried out with electrodes in liquid and solid state "solutions;" consider, for instance, the operation of chemical batteries, the electrolysis of alkali halide salts into their elements, the electroplating and electroforming of metals, or the production of metallic aluminum via the Hall process. Electrochemical gas reactions, though less common, are not unknown; H_2/O_2 fuel cells, electrical discharges for the production of ozone and the fixation of nitrogen, and magnetohydrodynamic power generation are examples. Commercial electrodes are traditionally fabricated from metals or carbon, but with advances in materials science, organic and semiconductor electrodes have become increasingly studied. Industrial electrodes are usually macroscopic in size, but their sizes have followed suit with micromanufacturing and nanomanufacturing practices.

Microscale and nanoscale electrode-mediated gas-phase reactions, such as those to be discussed in this paper, are interesting for several reasons, including the following.

(1) The current and projected importance of micron and submicron chemical devices merits deep understanding of gas and ion electrode physics at these small scale lengths.
(2) From a purely academic standpoint, the gas phase can obviate confounding solvent effects, exposing more clearly molecule and ion surface interactions, as well as reactions in the gas phase, thereby simplifying theoretical and experimental analyses.
(3) In the number density regime where the gas mean-free path is an appreciable fraction of the electrode separation distance, gaseous ions can be accelerated by electrode gap electric fields to many times their original thermal energies (i.e., $qV_b \gg kT$, with q ion charge, V_b the bias voltage, and kT the thermal energy). For example, if a room temperature gas-phase ion is accelerated through merely 1 V of potential, when thermalized it will achieve an effective temperature of $T \simeq 12\,000$ K. Thus, gas-phase electrochemical reactions involving ions, even at relatively low biasing, can make experimentally accessible a broad range of temperatures by which a variety of new reaction channels become possible. In tabletop apparatuses between microelectrodes, one can conduct chemical and plasma research at temperatures easily in excess of 10^6 K involving negligible energy input or heat loading.
(4) Electric field strength scales as $|\mathbf{E}| \sim V_b/x_g$; therefore, narrow gaps x_g favor strong fields. Since electrostatic energy density scales superextensively with E, V_b, and x_g ($\rho_E = (\epsilon_0/2)E^2 \sim \epsilon_0 V_b^2/2x_g^2$, where ϵ_0 is the permittivity of free space), narrow electrode spacing is desirable from an energy density standpoint.
(5) Narrow electrode spacing allows for high gas number densities n_g to be employed while still maintaining the long mean-free path criterion ($\lambda \geqslant x_g$) required for large individual ion energies and temperatures at relatively low biases.[4] By adjusting either x_g or n_g, one can tune the relative gas phase versus gas-surface collision frequency, as well as their relative kinetic energies and

[a)]FAX: 619-260-6874. Electronic mail: dsheehan@sandiego.edu

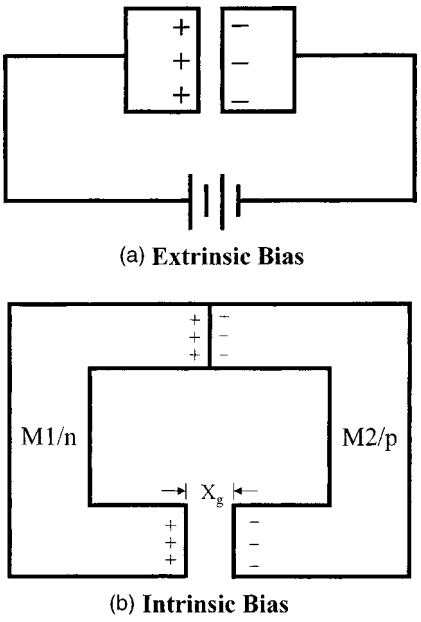

FIG. 1. Electrical biasing of metal and semiconductor electrodes: (a) extrinsic bias; (b) intrinsic bias. M1/M2 indicate metal types; n/p specify semiconductor doping types.

temperatures. For example, at standard temperature and pressure (STP) the mean-free path is about $\lambda \sim 7 \times 10^{-8}$ m; thus, if microelectrodes are separated by $x_g \sim 3 \times 10^{-7}$ m and biased at $V_b \sim 1$ V, then gaseous ions can achieve maximum energies of $qV_b \sim 1$ eV $\rightarrow 12\,000$ K and still undergo significant numbers of high-energy (or high-temperature) ion-neutral collisions in the electrode gap.

(6) Since surface area to volume ratio increases with decreasing object size, one expects high chemical reactivity per unit volume for micron and submicron sized catalysts.

In this paper we explore the basic physics of an electrochemical approach to catalysis that combines aspects of traditional catalysts with gas-phase electrodynamics, electrochemistry, and nanotechnology. In particular, we focus on the physics and chemistry of neutral and ionic gases on and between biased microscale and nanoscale semiconductor and metal electrodes. We consider surface-mediated ionization of neutral molecules, their acceleration to superthermal energies ($qV_b \gg kT$), and their prospects for high-energy gas-phase and gas-surface reactions.

The mode of electrode biasing fundamentally distinguishes the type of catalysis we introduce. Electrodes can be biased extrinsically or intrinsically, as depicted in Fig. 1. Traditional electrodes are biased extrinsically [Fig. 1(a)]; that is, they require an external voltage source. *Extrinsic bias* is effectively limited by the construction of the external voltage source as well as by considerations such as vacuum breakdown, tunneling, and the dielectric strength of the electrode. In contradistinction, *intrinsic bias* [Fig. 1(b)] requires no external voltage source, but rather, can arise simply by physically connecting two different solids having differing chemical potentials with respect to their charge carriers. Intrinsic bias can be established by connecting two pieces of semiconductor having different doping types or doping concentrations, or by joining two metals having different work functions [Fig. 1(b)]. The magnitude of intrinsic bias is limited to a maximum of a few volts, while extrinsic bias can be thousands or millions of times greater; however, given narrow electrode gaps, intrinsic bias can still render substantial electric fields. Also, since as a rule of thumb 1 eV translates into a temperature of $T \simeq 11\,600$ K, just a few electron volts can be sufficient to investigate most relevant high-temperature chemical (and many plasma) regimes. This *intrinsically biased electrocapactive catalysis* (IBEC) should be of both theoretical and practical interest.

More generally, intrinsic bias offers possibilities in the context of bias-driven nanochemistry and beyond. From a fundamental perspective it provides a link with naturally occurring gradient-driven processes in living bodies. From a practical perspective it suggests a number of applications, including the means to (a) power future nanodevices without resort to (macroscopic) external bias sources; (b) control microscopic charged particle beams; and (c) separate and manipulate dielectric nanoparticles via electric field gradients. Additionally, given that the attainable energies are sufficient for electronic and rovibrational population inversions in atoms and molecules, the potential for gas chemical lasers exists, if other lasing criteria can be met (e.g., gain length and high number density).

In the remainder of this paper we develop the theory of IBEC. We begin in Sec. II with a description of intrinsic biasing for metals and semiconductors, followed by electrocapacitive energy storage by catalyst particles. In Sec. III, positive and negative ion formation on surfaces is considered, followed in Sec. IV by general regimes of IBEC operation and a generic test case. In Sec. V prospects for experiments are considered and in Sec. VI thermodynamic issues are raised.

II. INTRINSIC BIASING

Intrinsic biasing occurs when materials possessing different chemical potentials with respect to their charge carriers are put into intimate physical contact. The relaxation of the chemical potential difference between the disparate materials promotes charge separation in the combined bulk, from which electric fields and potential differences result.[5] Below we examine intrinsic biasing in metals and semiconductors and show how they can give rise to a sizable equilibrium electric field in a vacuum gap, by which ions can be accelerated to superthermal speeds. The gap also stores appreciable electrostatic potential energy and, thus, can be considered an *intrinsic capacitor* of sorts.

In the following discussion, several types of potential will be introduced; for clarity we summarize them here: $V \equiv$ generic potential; $V_b \equiv$ externally provided bias potential; $V_c \equiv$ contact potential between disparate metals; and $V_{\mathrm{bi}} \equiv$ built-in potential between disparate semiconductors.

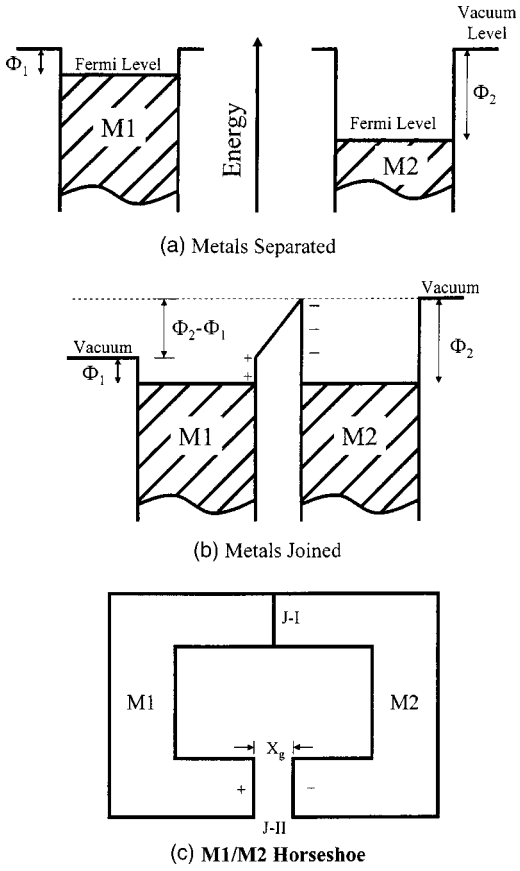

FIG. 2. Standard metallic device (SMD) and origin of intrinsic biasing. (a) Energy levels for two isolated metals showing disparate Fermi levels. (b) Energy levels for two connected metals, demonstrating common Fermi level but different vacuum levels. (c) Physical structure of horseshoe SMD.

A. Metals: Contact potential

To first approximation, a metal is a fluid of mobile electrons bound electrostatically and quantum mechanically in a lattice of positive ions. Because of Pauli exclusion, electron energies form a continuum, the Fermi sea [Fig. 2(a)]. The binding energy of the most weakly bound electrons (at the top of the Fermi sea) is the chemical potential of the metal or, more commonly, its work function Φ. Work functions for pure metals vary from less than 2 eV (e.g., Cs) up to about 6 eV (e.g., Pt).

When two metals are physically joined, so as to establish a uniform chemical potential throughout the bulk—that is, a single Fermi level, as indicated in Fig. 2(b)—electrons are transferred from the metal with the lesser work function Φ_1 to the metal with the greater work function Φ_2. As a result, the former metal M_1 charges positively and the latter metal M_2 negatively. A potential difference, the *contact potential* V_c, is established between the two metals: $qV_c \equiv \Phi_2 - \Phi_1$.

Consider the bimetallic device in Fig. 2(c), consisting of two mirror-symmetric horseshoe-shaped pieces of different metals (with differing work functions) facing one another. At junction I (*J*-I) the metals are physically connected, forming a standard metal-metal contact, while at junction II (*J*-II) there is a vacuum gap whose width x_g we take small compared to the length scale of the device x_{dev}; that is, $x_g \ll x_{\mathrm{dev}}$ such that the parallel plate approximation holds in the gap. Let $x_{\mathrm{dev}} = 10^{-6}$ m, and $x_g = 5 \times 10^{-8}$ m, $\Phi_1 = 5$ eV, $\Phi_2 = 4$ eV, so that $V_c = 1$ eV. The device with these parameters will be called the *standard metallic device* (SMD).

In addition to the electric field in *J*-I metal junction, a second electric field must be present in vacuum gap *J*-II. This can be deduced from Kirchhoff's loop rule or via Faraday's law. Kirchhoff's loop rule is an outcome of conservation of energy. Consider a closed vectorial loop threading the *J*-I region, the bulk of the device, and the *J*-II gap. Conservation of energy demands that a test charge conveyed around this closed path will undergo zero net potential drop; therefore, to balance the V_c drop across the *J*-I contact region, there must be a counterpotential elsewhere in the loop. Since, at equilibrium, away from the contact region there cannot be a potential drop in the bulk metal—otherwise there would be a nonequilibrium current flow, contradicting the assumption of equilibrium—the potential drop must occur outside the metal; thus, it must be expressed across the vacuum gap. Faraday's law ($\oint \mathbf{E} \cdot d\mathbf{l} = 0$) also establishes this result. The existence of the *J*-II gap electric field is well founded both experimentally and theoretically.

While the potential drop across the *J*-II vacuum gap is fixed to be $V_c = (\Phi_2 - \Phi_1)/q$, the electric field $\mathbf{E}$ depends critically on the *J*-II gap width: $|\mathbf{E}| = V_c/x_g$. [This assumes that x_g is not so narrow as to induce dielectric breakdown, field emission, physical electrostatic disruption, electrode-electrode tunneling, or other high-field effects, which can reduce $|\mathbf{E}|$. For the SMD, the field strength ($|\mathbf{E}| = V_c/x_g = 2 \times 10^7$ V/m) is far below that required for high-field effects.]

B. Semiconductor: Built-in potential

Consider a *p*-*n* device [Fig. 3(a)] of similar construction to the SMD, consisting of two mirror-symmetric horseshoe-shaped pieces of *n* and *p* semiconductor facing one another. At junction I (*J*-I), the *n* and *p* regions are physically connected forming a standard *p*-*n* junction, while at junction II (*J*-II) there is a vacuum gap whose width x_g we take small compared to the length scales of either the depletion region x_{dr} or the overall device x_{dev}; that is, $x_g \ll x_{\mathrm{dr}} \sim x_{\mathrm{dev}}$. Let the *n* and *p* regions be uniformly doped; the *p*-*n* junction is taken to be a step junction (graded junctions render similar results); diffusion of donor *D* and acceptor *A* impurities is negligible; the depletion approximation holds; impurities are completely ionized; the semiconductor dielectric is linear. For a silicon device as in Fig. 3(a), representative physical parameters meeting these conditions are $N_A = N_D = 10^{21}$ m^{-3}, $x_{\mathrm{dev}} = 10^{-6}$ m, and $x_g = 3 \times 10^{-8}$ m. The *p*-*n* device with these parameters will be called the *standard semiconductor device* (SSD).

When individual *n* and *p* materials are joined, charge carriers cross diffuse between the *n* and *p* regions forming the depletion region, whose width can range from 10 μm for a lightly doped semiconductor to 0.01 μm for a heavily doped one.[6] Space charge separation gives rise to a built-in potential (typical values, $V_{\mathrm{bi}} \sim 1$ V) and an internal electric field which arrests further charge diffusion. Standard one-dimensional formulas,[7]

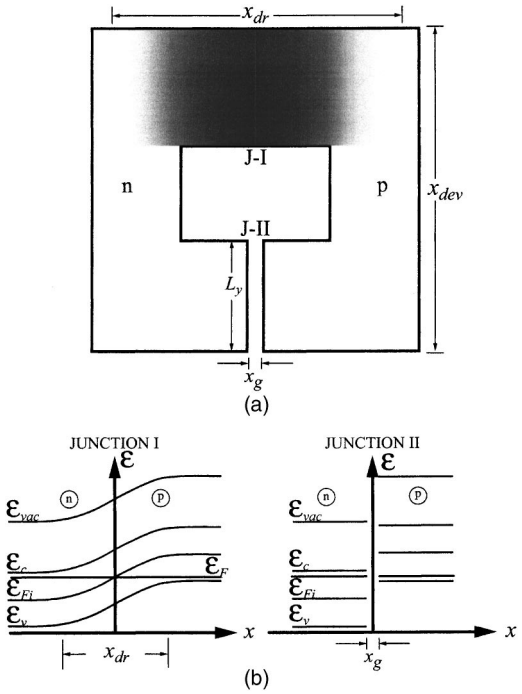

FIG. 3. Standard semiconductor device (SSD). (a) Physical schematic with gap and depletion region shown. (b) Physical characteristics vs position x through junctions I and II. Left ($x<0$) and right ($x>0$) sides of each graph corresponds to n and p regions, respectively. Legend: Energy levels for vacuum $\varepsilon_{\mathrm{vac}}$, conduction band edge ε_c, intrinsic Fermi level $\varepsilon_{\mathrm{Fi}}$, Fermi level ε_F, and valence band edge ε_v.

$$V_{\mathrm{bi}} = \frac{kT}{q}\ln\left(\frac{N_A N_D}{n_i^2}\right), \quad x_{\mathrm{dr}} = \left[\frac{2\kappa\epsilon_0 V_{\mathrm{bi}}}{q}\frac{(N_A+N_D)}{N_A N_D}\right]^{1/2}, \quad (1)$$

predict $x_{\mathrm{dr}}=1.2\times10^{-6}$ m and $V_{\mathrm{bi}}\simeq0.6$ V for the SSD. Here n_i is the intrinsic carrier concentration of silicon ($n_i\simeq1.2\times10^{16}$ m^{-3} at 300 K) and $\kappa=11.8$ is silicon's dielectric constant.

Across the *J*-I region [depicted in left frame of Fig. 3(b)], physical properties vary continuously with position, but across the open-gap *J*-II there are marked discontinuities in energy, voltage, and charge because of charge carriers' inability to jump the vacuum gap x_g, thus frustrating charge diffusion which would otherwise spatially smooth physical properties. Similarly as for the SMD, there can be large *J*-II gap electric fields ($E_{J\text{-II}}\sim V_{\mathrm{bi}}/x_g$), more than an order of magnitude greater than in the *J*-I depletion region. An electric field must exist in the *J*-II gap at equilibrium, just as for the metallic case. For the SSD, $|\mathbf{E}|=0.6\ V/3\times10^{-8}$ m$=2\times10^7$ V/m; thus, the SMD and SSD can support comparable electric fields.

Two-dimensional numerical simulations of the equilibrium states of the SSD were performed using Silvaco International's semiconductor Device Simulation Software [Atlas (S-Pisces, Giga)]. Output from the numerical simulations were two-dimensional, simultaneous, equilibrium solutions to the Poisson, continuity, and force equations, using the Shockley–Read–Hall recombination model. Over a wide range of experimental parameters ($10^{17}\leq N_{A,D}\leq10^{26}$ m^{-3}; $10^{-8}\leq x_g\leq3\times10^{-7}$ m), the two-dimensional numerical simulations showed good agreement with the primary findings of this one-dimensional (1D) analytic model, most notably, that large electric fields can reside in the *J*-II vacuum gap.

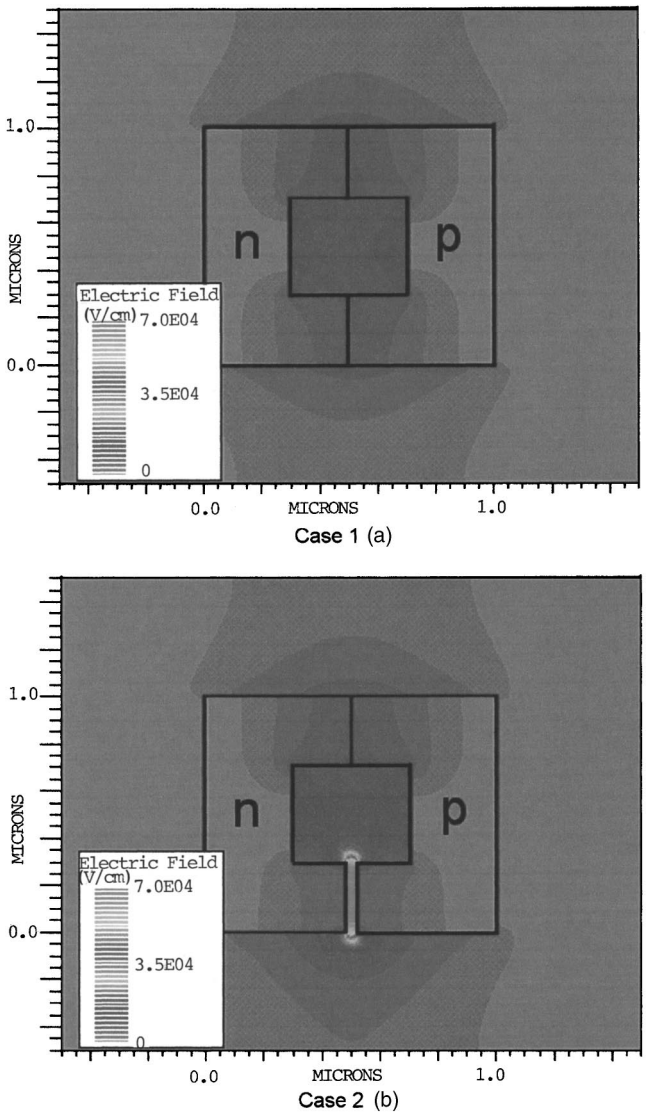

FIG. 4. Atlas 2D numerical simulations of electric field for closed-gap (a) and open-gap (b) configurations of the standard semiconductor device. [Electric field is linearly color graded from 0 V/cm (magenta) to 7×10^4 V/cm (orange-red). Note: Units are V/cm and μm.]

Figure 4 displays the electric field magnitude for the open- and closed-gap configurations of the SSD. As expected, the electric fields for the closed state [case 1, Fig. 4(a)] are modest ($|\mathbf{E}|\leq10^6$ V/m) and are centered on the depletion regions, which, as predicted in the 1D model, extend over the length of the device. While the electric fields in the *J*-I depletion regions of two cases are similar, in the *J*-II regions they are significantly different. The *J*-II electric field for the open state is $E\simeq7\times10^6$ V/m [Fig. 4(b)] versus an average of $E\simeq5\times10^5$ V/m for the closed state [Fig. 4(a)]. Numerical integration of the electrostatic field energy over the entire region (vacuum and bulk) indicates the total electrostatic energy of the open-gap case is roughly 1.5 times that of the closed-gap case. Considering only the *J*-II region of each device, the open state stores roughly twice the electrostatic energy of the closed state.

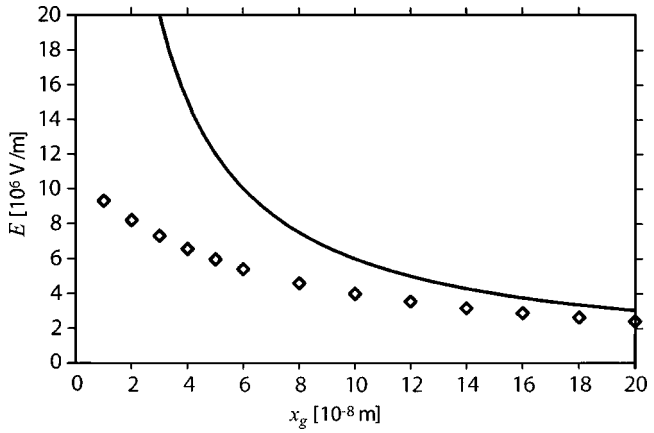

FIG. 5. Electric field strength for standard semiconductor device vs gap width x_g calculated at geometric center of *J*-II region for 1D analytic model (solid line) and 2D numerical model (open diamonds).

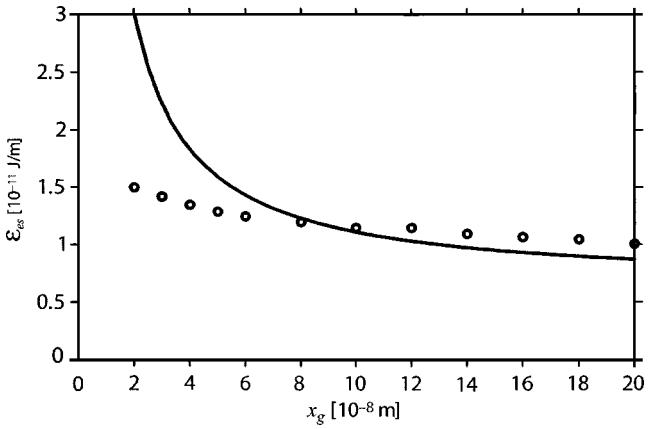

FIG. 6. Electrostatic potential energy $\varepsilon_{\mathrm{es}}$ vs gap width for standard semiconductor device [1D model (solid line); 2D model (open circles)].

In Fig. 5, the midchannel electric field is plotted versus gap width for the open-gap state of the SSD. Predictions of the 1D analytic model (solid line) are compared with results of 2D numerical simulations (open diamonds). The 1D analytic model overestimates the electric field compared with the 2D numerical simulation, particularly at small x_g, but this is expected given the 1D model's unphysical singularity at $x_g=0$. At small gap widths the 1D model predicts that the electric field should vary strictly as $1/x_g$, whereas in the 2D model, the charge carriers in the bulk respond to the high fields, bleed into the bulk semiconductor (see Fig. 4.), and thereby moderate them. As a result, the 2D model consistently renders lower field strengths than the 1D model, saturating at roughly 10^7 V/m, safely below the dielectric strength of silicon. At larger gap widths the two models agree well. Similar trends are expected for the SMD with the exception of the field bleeding effect.

C. Intrinsic capacitive energy

Electric fields store electrostatic potential energy with density $\rho_E=(\epsilon_0/2)E^2$. Capacitors are reservoirs for electrostatic energy, storing charge at an electrostatic potential. While capacitance is a geometric/compositional quantity inherent to the capacitor itself, charge, potential, and capacitive energy are normally set by an *extrinsic* work source. An *intrinsic capacitor* derives its electrostatic energy not from extrinsic work, but instead from intrinsic thermal processes (e.g., charge carrier diffusion, creation, and recombination), from which its contact or built-in potential is established. Furthermore, whereas standard capacitors dissipate their electrostatic energy through internal parasistic resistance R_i on a time scale $\tau\sim R_iC$, intrinsic capacitors can remain energized indefinitely. As such, they can be microscopic reservoirs of ready energy to power electrochemical reactions.

Capacitive energy storage $\varepsilon_{\mathrm{es}}$ for the metallic IBEC can be estimated from the standard formula for metallic capacitors:

$$\varepsilon_{\mathrm{es}}=\frac{1}{2}CV^2=\frac{1}{2}\frac{\epsilon_0 A}{x_g}V_c^2\simeq\frac{\epsilon_0 x_{\mathrm{dev}}^2}{2x_g}V_c^2=\frac{\epsilon_0}{2}E^2x_{\mathrm{dev}}^2x_g, \tag{2}$$

where the area A of the plates is taken to scale with the device size; that is, $A\simeq x_{\mathrm{dev}}^2$. Note that $\varepsilon_{\mathrm{es}}$ does not scale linearly with E or V_c; it is thermodynamically superextensive.

Theoretical limits to the capacitive energy available for the semiconductor case (SSD) are a bit more involved and can be estimated from the total electrostatic energy $\varepsilon_{\mathrm{es}}$ inherent to the *J*-II junction [Fig. 3(a)]. Let $\Delta\varepsilon_{\mathrm{es}}(J\text{-II})$ be the difference in electrostatic energy in *J*-II between its closed- and opened-gap equilibrium states. Within 1D model constraints, this is,

$$\Delta\varepsilon_{\mathrm{es}}(J\text{-II})\simeq\frac{\epsilon_0}{2}\left[\frac{x_{\mathrm{dr}}kT}{q}\ln\left(\frac{N_AN_D}{n_i^2}\right)\right]^2\left[\frac{1}{x_g}-\frac{1}{3}\frac{\kappa}{x_{\mathrm{dr}}}\right]. \tag{3}$$

Eliminating V_{bi} and x_{dr} with Eq. (1) and setting $N_A=N_D\equiv N$, Eq. (3) can be recast as

$$\Delta\varepsilon_{\mathrm{es}}(J\text{-II})\simeq\frac{16\kappa\epsilon_0^2}{qN}\left\{\frac{kT}{q}\ln\left[\frac{N}{n_i}\right]\right\}^3\times\left\{\frac{1}{x_g}-\frac{2}{3}\kappa\left(\frac{2\kappa\epsilon_0}{Nq}\left(\frac{kT}{q}\right)\ln\left[\frac{N}{n_i}\right]\right)^{-1/2}\right\}. \tag{4}$$

Equation (3) predicts that the open *J*-II region can store significantly more electrostatic potential energy than the closed *J*-I region;[8] the *standard semiconductor device's J*-II region contains roughly three times the energy of the *J*-I region. In principle, this excess electrostatic energy can be released chemically. Thermodynamically, this may be viewed as simply the relaxation of the system from a higher energy (open-gap) to a lower energy (closed-gap) equilibrium state.

Potential energy is stored in the *J*-I and *J*-II regions of the intrinsic capacitor in both the open- and closed-gap configurations. In Fig. 6, the total device energy $\varepsilon_{\mathrm{es}}$ is plotted versus x_g for the SSD, comparing the 1D and 2D models.[9] The total electrostatic energy is the sum of the contributions from the vacuum energy density $(\epsilon_0E^2/2)$ and *n-p* bulk energy density $(\kappa\epsilon_0E^2/2)$, integrated over their respective regions. For both models, the device energy decreases mono-

tonically with increasing gap width, however, their magnitudes and slopes differ due to the differing model assumptions. At small gap widths ($x_g \leqslant 10^{-7}$ m), the 1D model predicts greater energy than the 2D model, owing principally to its vacuum energy, whereas at larger gap widths ($x_g \geqslant 10^{-7}$ m) the energy in the 2D model's *n*-*p* bulk dominates. (The 1D model explicitly ignores energy contributions from the *p*-*n* bulk on either side of the vacuum gap.) In the density vicinity of the SSD, the two models agree to within about 50%.

As for the metallic case, the SSD constitutes a high-energy equilibrium state, an intrinsically biased capacitor, which can remain charged indefinitely since the open-gap configuration is an equilibrium state of the system. In constrast to the SMD, however, the SSDs capacitive energy varies strongly with temperature—scaling as T^3 in Eq. (4)—since primary determinants of the energy are V_{bi} and x_{dr}, both of which derive from thermal processes. When T falls below the freeze-out temperature for the charge carriers (for silicon, $T_{\mathrm{freeze}} \leqslant 100$ K), charge diffusion ceases, the silicon becomes intrinsic, $V_{\mathrm{bi}} \rightarrow 0$, and the capacitive energy disappears; in effect, both the *n* and *p* regions become electrically identical to undoped silicon. Metals have no freeze-out temperatures.

In summary, it has been shown for both metallic and semiconductor cases that significant electrostatic potential, electric field, and potential energy can be stored in an open-gap IBEC, thereby constituting an energized microscopic capacitor.

III. POSITIVE AND NEGATIVE ION FORMATION

Neutral gas molecules X interacting with a surface can form positive or negative ions depending on the magnitudes and state multiplicities of the surface's and gas species' energy levels. For metal surfaces, the energy necessary for a molecule to desorb as a positive ion ($\Delta E^{+}_{\mathrm{des}}$) can be roughly estimated as[1,2,10]

$$\Delta E^{+}_{\mathrm{des}} \simeq \Delta E_{\mathrm{des}} + E_i - \Phi, \tag{5}$$

where ΔE_{des} is the desorption energy for the neutral molecule, E_i is the gas species' ionization energy, and Φ is the metal's work function. Prediction of surface ionization from a purely energetic standpoint is relatively straightforward: one compares the gas species' E_i and electron affinity E_{ea} to the metal's work function Φ. If $\Phi > E_i$, then the gas X is likely to lose an electron to the metal and desorb as a positive ion X^{+}. Conversely, if $E_{\mathrm{ea}} > \Phi$, then it is energetically favorable for the gas to attach an electron from the metal and desorb as a negative ion X^{-}. At equilibrium, the ratio of positive ionic j_i^{+} to neutral j_0 fluxes off a metal is given by the Saha–Langmuir equation:

$$\frac{j_i^{+}}{j_0} \equiv P_i = \frac{g_i}{g_0} \exp\left[-\frac{(E_i - \Phi)}{kT} \right], \tag{6}$$

where g_i/g_0 is the ratio of statistical weights for the ionized and neutral states of the gas. For negative ion formation, $(E_i - \Phi)$ is replaced with $(\Phi - E_{\mathrm{ea}})$. Desorption can be augmented by high temperatures. Aside from alkali metals and alkali earth metals, which have small ionization energies, most molecules are not disposed toward positive surface ionization and desorption except at relatively high temperatures, where they are often susceptible to thermal disintegration. Negative surface ionization is similarly restricted outside a small set of halogen related compounds. On the other hand, select organic molecules can form relatively stable positive and negative ions—carbocations and carbanions—when stabilized by charge delocalization through conjugated bonds, aromaticity, resonance structures, or by appropriate electron-donating or withdrawing moieties. (Charge delocalization can also aid surface desorption by propitiously separating a molecule's charge from its image charge in the surface.) Well-known examples include fullerenes, which via delocalization can bear either net negative or positive charge, and the cyclopentadienyl anion and tropylium cation which are aromatically stabilized.[11]

A process closely related to IBEC at high temperatures ($T \geqslant 1500$ K) is surface-mediated plasma production resulting from simultaneous surface ionization of a gas and electron thermionic (Richardson) emission. The classic example is the *Q* plasma, which has been studied extensively theoretically and experimentally for over 40 years.[12,13] *Q* plasmas are traditionally produced by contact surface ionization of an alkali metal (e.g., K, Rb, Cs) or alkali earth metal (e.g., Sr, Ba) on a high-temperature ($T = 2000$–2500 K), high-work function, refractory metal surface (e.g., Mo, Ta, W, Re). The heated metal thermionically emits electrons. For an electron-rich plasma, the negative electron space charge over the metal accelerates the ions superthermally off the metal surface, up to several times the ion thermal speed. Meanwhile, the positive ion flux relaxes the space charge restriction on electron flow; thus, they leave together as a nearly neutral electron-ion plasma. In *Q* plasmas, the electrons are basically thermal, while the ions leave as a superthermally drifting, half-Maxwellian distribution that usually relaxes quickly to a drifting full-Maxwellian via gas-phase collisions. Ion number densities in excess of 10^{19} m^{-3} have been achieved.

More exotic *Q* plasmas, in which electrons are almost completely replaced by negative ions, have also been studied.[14,15] These are produced by thermal ionization of alkali halide salts (e.g., CsI, KI) on heated refractory metals or ceramics (e.g., Al_2O_3, ZrO_2). Electrons have also been removed from standard *Q* plasmas by gaseous electron scavengers such as SF_6 and WF_6, which have large electron affinities and large electron capture cross sections near *Q*-plasma electron thermal energies ($kT \simeq 0.2$ eV).[15,16] These various traditional and exotic *Q* plasmas offer insights into the experimental possibilities for IBEC.

On semiconductors, ion production is more subtle than on metals and lends itself more to quantum mechanical treatment owing to the more discrete nature of surface energy states. Nonetheless, the concepts of work function, ionization energy, desorption energy, and electron affinity carry over from the metallic to the semiconductor case such that one expects analogous ionization and desorption behaviors.

Overall, metallic IBECs would seem to have several advantages over semiconducting ones. First, owing to their higher electrical conductivity, the free charges on the *J*-II metal electrode faces are more smoothly distributed and

more quickly restored than in the semiconductor case. Second, refractory metals (e.g., Ta, W, Ir, Os, Mo), many of which are already staples of the catalytic industry, can survive higher temperatures than most standard semiconductors, making them more suitable for high-temperature operation. High temperatures favor desorption of adsorbed species, electron thermionic emission, and baking out of catalytic poisons. Third, the maximum work function differences between metal pairs can be greater than those achievable between differentially doped semiconductors. For example, the built-in potential for silicon *p-n* junctions is typically about 1 V or less, while for select metal electrode combinations the contact potential can be several times larger; for instance, a Pt–Ca contact potential is roughly 4 V. Finally, the metallic *J*-II gap can probably sustain larger maximum equilibrium electric field strengths than the semiconductor case. Whereas equilibrium electric fields are forbidden inside bulk metal beyond the skin depth, up to the dielectric strength of the metal itself, numerical simulations show that large electric fields tend to bleed into bulk semiconductor well below its dielectric strength [Fig. 4(a)], thereby imposing an upper limit *J*-II gap electric field strength of about 2×10^7 V/m. Thus, we hold that metals are advantageous IBEC candidates.

IV. OPERATIONAL REGIMES AND TEST CASE

The IBEC effect should be viable across a broad range of physical parameters, making a general analytic treatment infeasible. Here we identify limiting regimes of operation and sketch some general operating parameters through a qualitative discussion.

The *J*-II electric field implies that apposing gap surfaces are charged positively and negatively. This charge might aid surface reactions, e.g., by modifying molecule-surface states, perhaps via electron withdrawl or donation, or by molecular polarization. Thus, surface charge itself—not simply gaseous ions—might play significant roles in IBEC. This will be considered in future studies; here we concentrate on ion energization and its ramifications.

Once desorbed and clear of surface potentials, ions are accelerated by the gap electric field. Depending on the type and number density of the gap gases, one can imagine a number of possible reaction channels. The ions themselves might be the chemically reactive species of interest or they might affect the reactivities of other species. Possible reaction channels are numerous, but here we concentrate solely on ions as *molecular projectiles*. In this role, ions might impart their superthermal kinetic energy to adsorbed species, thereby opening new surface reaction channels; they might collide with or heat the intervening gas, thereby facilitating gas-phase reactions; or they might bombard chemisorbed or physisorbed species on the opposite electrode, thereby facilitating surface desorption. Most physical chemical processes attributed to low-energy ion beams ($E\leqslant 4$ eV) should be possible via IBEC.[17]

Alkali metals and halogens appear to be ideal candidates for X^+ and X^- molecular projectiles since they have relatively low ionization energies and high electron affinities, respectively; they are also relatively disinclined toward fragmentation. Similarly as for *Q* plasmas, alkali halide salts might be fruitful candidates, producing both types of ions simultaneously.[14,15]

At least three general regimes of operation can be identified for IBEC on the basis of the relative magnitudes of the gas mean-free path λ and the *J*-II gap width x_g.

Regime I: ($\lambda\gg x_g$). At low gas number density, the mean-free path can greatly exceed the electrode separation, $\lambda\gg x_g$. For the SSD/SMD this would correspond to gas number densities less than about $n_g\simeq10^{24}$ m^{-3}. In this regime, relatively few gas-phase collisions or reactions are expected. Rather, most gas ions are expected to fall through the full gap potential V_b before striking the opposite electrode. If the ions rebound and thermalize, one expects a high temperature gas or plasma to develop in the gap. In this regime, the neutral gas and ions are likely to be only a minor perturbation to the gap's electrostatic potential and field.

Regime II: ($\lambda\sim x_g$). At intermediate gas density, where the mean-free path is comparable to the electrode separation, appreciable levels of both ion-neutral and ion-surface collisions are expected. Because of gas-phase collisions, ion energies should span roughly the range $kT_0<E_{\text{ion}}<kT_0+qV_b$, where T_0 is the initial temperature. Likewise, the temperature T of the neutral gas should be boosted by collisions into the range $T_0<T<T_0+qV_b/k$. As the gas density is increased, the gas temperature and ion energy should decrease since the finite electrocapacitive energy is shared among more particles. Also, as significant numbers of ions are generated, these should affect the gap electrodynamics, possibly neutralizing the electric field which, in turn, should reduce ion energy and temperature.

Regime III: ($\lambda\ll x_g$). At high gas density the mean-free path can be significantly less than electrode separation. In this regime, ions suffer multiple collisions crossing the gap and their individual energies are much reduced from their theoretical maximum; i.e., one expects $E_{\text{ion}}\ll qV_b$. On the other hand, this energy is not lost; rather, it is collisionally dissipated as heat, raising the temperature of the bulk background gas above T_0. This regime might be conducive to reactions that are sensitive to smaller temperature changes and which do not require, or cannot tolerate, high energy ions. At these high number densities, the electrodynamics of the cavity might be severely altered by the ion populations. In the extreme, the electrodes might become sufficiently covered with adsorbed gas so as to shut down the intrinsic biasing mechanism, in which case the electrocatalytic activity would cease.

A heuristic graph summarizing the above relationships between λ, n_g, T, and E_{ion} in regimes I–III is given in Fig. 7. At either graphical extreme, $|\log(\lambda/x_g)|\equiv|N|\gg1$, the behavior of the system saturates. In the $N\gg1$ regime (regime I) ions are energetic (corresponding to high temperature), but there are few of them, while at the opposite extreme ($N\ll0$, regime III), there are many low-energy ions and the temperature is near T_0. One suspects that somewhere between these extremes the chemical activity might be optimized, perhaps somewhere in the mid-range of the sigmoid, near $N=0$, suggestive of regime II.

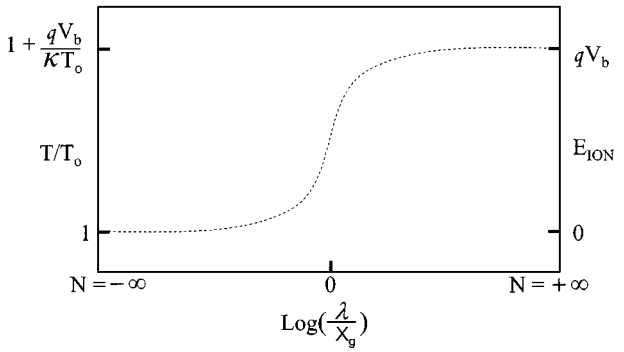

FIG. 7. Heuristic graph of interrelationships of mean-free path λ, electrode separation x_g, temperature T, and ion energy E_{ion} for the IBEC, where $N \equiv \ln(\lambda/x_g)$. Operating regimes: regime I ($N \gg 1$); regime III ($N \ll 1$); and regime II ($N \sim 0$).

A general analytic description of IBEC is not possible, but given adequate physical and chemical parameters, individual systems are amenable to numerical simulation. Although a system would seem to be fully specified by its geometric construction, choices of electrodes and gas species, temperature, and number densities, this belies its true complexity. One should have full accounting and specifications of all gas-phase and gas-surface reaction channels and their mutual feedbacks; in turn, these must be incorporated into plasma or fluid codes (or their equivalent in the high Knudsen number regime) and processed in a time-dependent, dynamic manner. Like many nonequilibrium systems, the IBEC is likely to behave nonlinearly and, thus, will be sensitive to initial conditions. As a result of these complexities, here we only sketch some broad lines of practicality rather than attempt to paint a detailed picture.

A. Test case: Spool

The optimal geometry for an IBEC cell depends on its specific application. In Fig. 8 is presented one simple design, termed the *spool*, which embodies several generally desirable features. The spool is constructed from M1/M2 or n/p cylindrical pairs of diameter x_{cell}, joined on axis, and is of similar size to the SSD/SMD. The electrode spacing is relatively narrow compared with the device dimensions, allowing for relatively uniform and intense gap electric fields, but the geometry is such that neutral gas can flow into and out of the electrode gap radially over broad area and direction.[18] The device's surface-to-volume ratio is good; each cell has roughly x_{cell}^2 electrode surface area.[19] The spool is encased by an electrical insulator to make it electrically independent of other cells [Fig. 8(b)]. Also, in this design, the insulation thickens the electrode walls and impedes interlocking with other cells. These cells might be stacked axially into larger structures, or left jumbled such that gas might diffuse through a bed of them. If $x_{\mathrm{cell}} \simeq 10^{-6}$ m, the reactive surface area to volume ratio for a spool is roughly 4–5 $\mathrm{km}^2/\mathrm{m}^3$ (neglecting dendritic surfacing of the electrodes). The inner electrode surfaces might be scalloped and insulated, as depicted in Fig. 8(c), so as to increase local electric fields and concentrate chemical activity toward the scallop points.

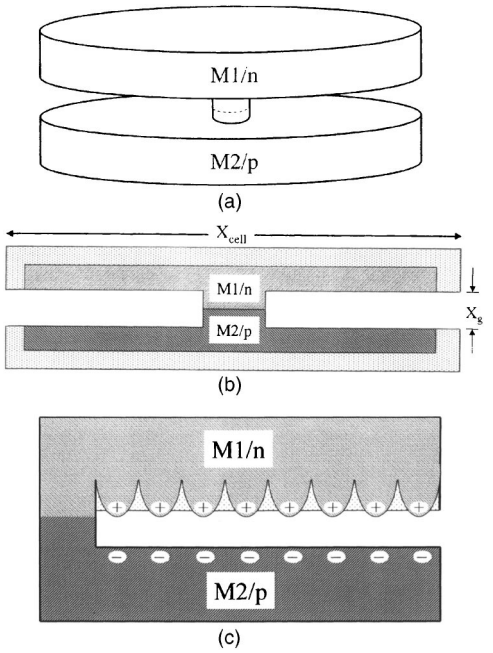

FIG. 8. Spool IBEC cell. (a) Perspective sketch. (b) Side view, cut through axis. (c) Scalloped inner electrode surfaces. Legend: metal (darker grays), electrical insulator (light gray stipple).

If the electrostatic energy content of an electrocatalytic cell is ε and if its discharge/recharge time is τ_{dr}, then a measure of the maximum instantaneous electrostatic power deliverable by a single cell is $P_{\mathrm{cell}} \sim \varepsilon/\tau_{\mathrm{dr}}$. If the particle flux of reactants through the cell is $\mathcal{F}(\mathrm{s}^{-1})$, then the available electrostatic energy per reactant molecule is given dimensionally by $\varepsilon/\tau_{\mathrm{dr}}\mathcal{F}$. Let the cell size scale be x_{cell} and let the scale size of the catalytic bed be L_{bed}. Depending on the gas flow regime, the cell packing structure, and the bed plumbing, the average number of cells visited by a molecule on its travel through the bed will vary considerably. At one extreme, where a low number density (lightly collisional) gas jets ballistically through the catalytic bed packed with uniformly arrayed cells in a highly directional manner, one expects a minimum number of gas-surface collisions, N_{ball}, here taken to be of the order of $N_{\mathrm{ball}} \sim L_{\mathrm{bed}}/x_{\mathrm{cell}}$. At a different extreme, where a high number density (highly collisional) gas meanders through a convolutedly plumbed bed, packed with randomly oriented cells, the gas flow is essentially diffusive, in which case the number of gas-surface collisions should scale more closely to that of standard gaseous diffusion: $N_{\mathrm{diff}} \sim (L_{\mathrm{bed}}/x_{\mathrm{cell}})^2$. (This assumes x_{cell} represents the gas mean-free path.) For the former, conservative ballistic flow case, the theoretical electrostatic energy per reactant molecule available during its passage through the bed χ can be estimated dimensionally as

$$\chi \sim \frac{\varepsilon N}{\tau_{\mathrm{dr}}\mathcal{F}} = \frac{\varepsilon L_{\mathrm{bed}}}{\tau_{\mathrm{dr}}\mathcal{F}x_{\mathrm{cell}}}. \tag{7}$$

Qualitative estimates can be made for realistic physical systems. Consider a standard spool constructed from the combination M1/M2=Ta/Re (Ta:mp=3287 K, $\Phi_{\mathrm{Ta}} \simeq 4$ eV; Re:mp=3453 K, $\Phi_{\mathrm{Re}} \simeq 5$ eV) with alumina electrical insulation (Al_2O_3:mp $\geqslant$ 2000 K). Let $x_{\mathrm{cell}}=10^{-6}$m and $x_g=5$

$\times 10^{-8}$ m, similarly as for the SMD/SSD, so that $V_c \simeq 1$ V and $E \simeq 2 \times 10^7$ V/m. In this case, an individual spool cell stores $\sim 10^{-16}$ J of electrostatic energy and its discharge time τ_{dr} should be short, on the order of $\tau_{dr} \simeq 10^{-7}$—10^{-8}s, consistent with typical inverse slew rates of micron-sized *p-n* diodes or the *RC* time constants of microscopic capacitors. In this case, the instantaneous power for a single, switched cell should be $P_{cell} \simeq 10^{-9}$–10^{-8} W. Instantaneous power densities ($\mathcal{P}_{cell}$) can be large; for the spool, $\mathcal{P}_{cell} = P_{cell}/(10^{-6}\ \text{m})^3 \sim 10^9$–$10^{10}$ W m^{-3}. Presuming gas density at STP that flows sonically, one estimates the molecular flux through the spool to be $\mathcal{F} \simeq 10^{15}$ s^{-1}. Let $L_{bed} = 1$ m and $x_{cell} = 10^{-6}$ m, such that $N \simeq 10^6$. With these, one finds from Eq. (7) that, on average, $\chi \simeq 10^{-18}$–10^{-17} J $\simeq$ 6–60 eV is available per molecule on its journey through the catalytic bed. This is adequate to drive chemical reactions, even allowing for thermodynamic inefficiencies.

V. EXPERIMENTAL OUTLOOK

Experimental tests of the IBEC concept are under consideration. Catalytic activity and selectivity can be measured for IBEC cells with different M1/M2 pairings, e.g., M1/M1 versus M2/M2 versus M1/M2, with the former two acting as controls. Suppose a surface reaction ($A+B \rightarrow C$) is catalyzed on M2 but not on M1. If $\Phi_2 > \Phi_1$, such that an electric field is directed from M1 toward M2, then by introducing a positively ionizable species X into the IBEC bed along with gases A and B, a superthermal flux of X^+ can bombard M2, augmenting gas or surface reactions. An efficacy test would consist of measuring reaction products from independent beds consisting of M1/M1, M1/M2, and M2/M2 catalysts, varying of course the usual thermodynamic parameters such as temperature, pressure, and gas ratios. If the M1/M2 is found superior to either M2/M2 or M1/M1 under otherwise identical conditions, this would be evidence (but surely not confirmation) of the IBEC effect.[20]

It is difficult to predict which reactions might most benefit from IBEC since catalysis is often a multivariable phenomenon. It would be particularly interesting to test IBEC beds at room temperature for reactions that normally proceed at elevated temperatures, thereby testing the anticipated effects of high local gas temperatures inside the catalytic cells. This assumes that the reactions require elevated *gas* temperatures, but not necessarily elevated *surface* temperatures.[21] Other tests can be envisioned. For example, hydrocarbon dehydrogenation reactions proceed well on Pt between about 450–750 K, while Ta is not known for comparable catalytic activity. The work functions of Pt and Ta are roughly $\Phi_W = 6.2$ eV and $\Phi_{Ta} = 4.2$ eV, so that a Pt/Ta IBEC spool cell would support a 2 V potential across its gap. If Cs is introduced as the ionizable working gas, the Langmiur–Saha equation (6) predicts virtually complete ionization to Cs^+ at $T = 600$ K on both Pt and Ta surfaces.[22] For the control catalysts, M1/M1 $\equiv$ Ta/Ta might have limited hydrogenative activity at 600 K, while for M2/M2 $\equiv$ Pt/Pt activity should be sizable. If superthermal Cs^+ boosts catalytic activity, perhaps by stimulating surface desorption of products or aiding reactants over activation barriers, the Pt/Ta IBEC could outperform Pt/Pt.

Surface area per unit mass (m^2/gm) is a standard figure of merit for catalysts. For example, the surface area/mass for finely divided Ni used for the hydrogenation of unsaturated glycerides is typically 25–40 m^2/gm, while for supported catalysts with significant porosity (e.g., silica gel, charcoal, zeolites, and γ alumina) values of 10^2–10^3 m^2/gm are not uncommon. IBEC cells could have area/mass ratios comparable to these. Insofar as IBEC requires two metals with well-defined work functions, one must have sufficient numbers of atoms to generate bulk properties (like Φ), thus putting a lower limit for cell size at about 10^{-8}–10^{-9} m. Additionally, the metals must be physically joined and must possess a plate geometry that fosters usable ion acceleration. Again this suggests a lower size limit of about 10^{-8}–10^{-9} m to be in line with current nano-fabrication techniques. Given this, and assuming mass densities of roughly $\rho \simeq 5$ gm/cm^3, one can show that with realistic dendritic or porous structures, the upper-limit area/mass ratio for IBEC cells is of the order of 10^2–10^3 m^2/gm, which is comparable to maximum values seen with commercial catalysts.[23]

VI. DISCUSSION

As developed in the previous sections, IBEC presents a potentially practical tool for nanochemistry—a hybrid between a typical catalyst and an electrochemical cell. On one hand, quite aside from the catalytic properties of M1 and M2 individually, IBEC appears capable of increasing reaction rates and opening new reaction channels, while not being consumed in the process and, at the end of the chemical event, resuming its original thermodynamic state; thus it satisfies the traditional criteria for a catalyst. More interesting, however, are thermodynamic issues surrounding its intrinsic bias and stored electrocapacitive energy, which shade its catalytic status.

For the IBEC effect to be viable, the system must be held significantly out of equilibrium with respect to gas flow. The high-energy ions and elevated temperatures predicted for the *J*-II gap are only transient conditions leading to equilibrium. When equilibrium is reached there will be little IBEC activity and in place of ionic fluxes from either side of the gap there will be a static gas-ion atmosphere. The number density of neutrals will be spatially uniform, while the density of ions will be exponentially stratified similarly as for a textbook isothermal gas atmosphere in a uniform gravitational field ($\rho = \rho_0 \exp[-mgz/kT]$), where z is altitude. In the gravitational case the potential energy of a gas atom is (mgz), whereas in the electrostatic IBEC case the potential energy of an ion is set by its x location in the gap: $[(qV_b/x_g)x]$. Positive ions will be stratified in the opposite direction as negative ions.[24] The various species' number densities in the gap are figuratively depicted in Fig. 9.

Equilibrium should be achieved rapidly, probably within a few to several thermal transit times across the gap, $\tau_{transit} = x_g/v_{th}$, where $v_{th} \simeq \sqrt{kT/m}$. For the SSD/SMD with $v_{th} \simeq 10^2$–10^3 m/s and $x_g = 5 \times 10^{-8}$ m, equilibrium should be achieved within about 10^{-8}–10^{-10} s, which, not surprisingly,

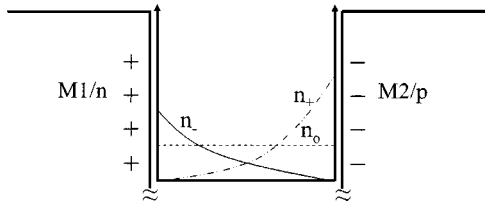

FIG. 9. Heuristic depiction of equilibrium number density vs position in electrode gap for positive, negative, and neutral gas species.

is roughly of the same order as the discharge time τ_{dr} for *p -n* diodes of comparable size. Note, however, that $\tau_{transit}$ is orders of magnitude longer than typical timescales for chemical reactions, which are usually comparable to the vibrational period of molecular bonds ($\tau_{vib} \sim 10^{-13}$ s); thus, one can expect significant chemical activity before charge balance and thermal equilibrium are attained.

In all, the short-lived, nonequilibrium stages of electrical discharge are conducive to the formation of high-energy ions and high temperatures. In theory, these transient nonequilibrium conditions can be fostered by intermittantly pulsing gas through the catalytic bed, as is common in *flow reactors* that feature large concentration gradients between bed entrance and egress.[3] Between pulses, the chemical products and residual reactants will clear the bed and the intrinsic capacitors will recharge.[25]

For reactions that are exothermic—for instance, the Haber process for ammonia synthesis on iron ($N_2 + 3H_2 \rightarrow 2NH_3$), IBEC is thermodynamically unsurprising since the reaction merely heats the catalyst; however, if the reaction is endothermic—for instance, coal gasification with steam into syn-gas ($coal + H_2O \rightleftharpoons CO + H_2$)—then an interesting thermodynamic issue emerges. Specifically, if the capacitive energy $[\rho = (\epsilon_0/2)E^2]$ is tapped either directly or indirectly to drive an endothermic reaction and if it appears as extra chemical energy in the products, then the IBEC appears capable of permanently shifting an equilibrium, quite unlike a classical catalyst.[26] While, superficially, the IBEC-driven reaction should be no more surprising than a electrochemical reaction driven by, let us say, a battery, things are not so simple. If the IBECs electrostatic energy is tapped, then when the reactants and products clear the catalytic bed, the catalyst's capacitive energy will rebuild to its prereaction equilibrium value—after all the recharged state is an equilibrium state. It appears that, in principle, IBEC electrostatic energy can be tapped again and again in this fashion to imbue reaction products with a net increase in chemical energy, but this raises the question: What is the source of this renewable electrostatic energy turned into chemical energy? At present the energy source is elusive, but without a particular and complete reaction cycle in mind, the question probably cannot be answered definitively. Given the novel hybrid nature of IBEC, perhaps it is not surprising that thermodynamic issues such as these arise. These will be the subject of future inquiry.

VII. SUMMARY AND CONCLUSIONS

Analysis and numerical simulations indicate an electrochemical approach to catalysis, wherein the electrostatic potential energy in open vacuum gaps under intrinsic biasing drives gas-phase and gas-surface chemical reactions via accelerated gaseous ions. A number of reaction channels are possible, but all occur during the short-lived nonequilibrium period during capacitive discharge of the catalyst. Employing gas pulsing through a catalytic bed of microscopic or nanoscopic catalytic cells, relatively high gas densities and throughputs might be possible. These catalysts potentially offer a number of attractive features, including respectable surface-to-volume ratios, high (but short-lived) energy and power densities, and high internal gas temperatures (in excess of 10^4 K), by which the need to bulk heat catalysts can be relieved.[27] Estimates based on realistic physical parameters indicate that the IBEC effect should be experimentally testable within the current arts of chemistry and nanotechnology.

Beyond the chemical applications of IBEC, intrinsic biasing suggests a number of additional applications. These include providing local power sources for future nanodevices; directing charged particle beams at the submicron level; sorting and collecting dielectric particles; and powering gas chemical lasers. Intrinsic bias represents a general scheme for creating appreciable electric fields ($|\mathbf{E}| \leqslant 10^7$ V/m) and field gradients, and for storing ready electrocapacitive energy at the submicron scale without need of external power sources.

ACKNOWLEDGMENTS

It is a pleasure to thank E. K. Perttu, J. H. Wright, and K. Adkins for their assistance in preparing figures for this paper. T.S. is grateful to the NSF (Grant No. CHEM/MRD-0313638) for support of this project. D.P.S. acknowledges the kind support of the Research Corporation and a USD Faculty Research Grant. Finally, both authors warmly thank V. Špička for the stimulating atmosphere at *Frontiers of Quantum and Mesoscopic Thermodynamics-04* (Prague, 2004), which led to the ideas presented in this paper.

[1] B. C. Gates, *Catalytic Chemistry* (Wiley, New York, 1992).
[2] G. A. Somorjai, *Introduction to Surface Chemistry and Catalysis* (Wiley, New York, 1994).
[3] *Catalyst Handbook*, 2nd ed., edited by M. V. Twigg (Wolfe, London, 1989).
[4] High n_g also allows large gas throughput.
[5] One can view intrinsic biasing as reflecting a trade-off between chemical and electrostatic potentials.
[6] In the limit of heavy doping, the semiconductor case (SSD) essentially reduces to the metallic case (SMD).
[7] G. W. Neudeck, in *The pn Junction Diode* 2nd ed., Modular Series on Solid State Devices Vol. II, edited by R. F. Pierret and G. W. Neudeck, (Addison-Wesley, Reading, 1989).
[8] ΔE_{es} in Eq. (3) is positive definite for $x_g \leqslant 3/\kappa x_{dr}$. For the silicon SSD this puts the following constraint on the gap width: $x_g \leqslant \frac{1}{4} x_{dr}$.
[9] Energy is normalized with respect to the *z* direction (J/m) so as to conform with the output of the 2D numerical model.
[10] R. I. Masel, *Principles of Adsorption and Reaction on Solid Surfaces* (Wiley, New York, 1996).
[11] P. J. Garratt, *Aromaticity* (Wiley, New York, 1986).
[12] R. W. Motley, *Q-Machines* (Academic, New York, 1975).
[13] N. Rynn and N. D'Angelo, Rev. Sci. Instrum. **31**, 1325 (1961).
[14] S. von Goeler, T. Ohe, and N. D'Angelo, J. Appl. Phys. **37**, 2519 (1966).

[15]D. P. Sheehan and N. Rynn, Rev. Sci. Instrum. **59**, 1369 (1988).
[16]A. Y. Wong, D. L. Mamas, and D. Arnush, Phys. Fluids **18**, 1489 (1975).
[17]These ion energies are below the threshold for sputtering, ionization or secondary emission from the apposing electrode, lattice dislocation, or implantation. They are sufficient, however, to excite translational, rotational, vibrational modes, and, in principle, chemical reactions.
[18]Ions tend to be trapped in the spool by gap fields, while neutrals can traverse the gap unimpeded.
[19]This can be increased with dendritic surface finishing.
[20]For instance, it might be the case that M1 produces intermediates that facilitate reactions on M2, irrespective of the gap electric field. Such processes would complicate verification of the IBEC effect.
[21]Often the gas and surface temperatures will not equilibrate on the time scale of the experiment.
[22]At this temperature, Cs has a high vapor pressure and Cs^+ should also have a reasonable desorption probability. In Q-plasmas, ion number densities in excess of 10^{19} m^{-3} have been demonstrated.
[23]Important concerns surrounding the catalyst's structural integrity, lifetime, and poisoning are beyond the scope of this discussion.
[24]One can view the gas ions in the *J*-II gap as performing a substitute role for the charge carriers in the *J*-I depletion region of the SSD. The gas *J*-II ions act to balance chemical and electrostatic potentials so as to establish a static, low-energy equilibrium state.
[25]A buffer gas (e.g., He, Ar) might accelerate this purging process.
[26]A catalyst cannot alter the chemical equilibrium of a reaction; it can only speed both forward and reverse reactions so as to achieve equilibrium more rapidly.
[27]It is remarkable to consider that, in principle, one could casually handle a room temperature catalyst, belying its 10 000 K interior gas temperature.